Influence of Gold Nanorod Geometry on Optical Response

Anthony S. Stender, Gufeng Wang, Wei Sun, and Ning Fang*

Ames Laboratory, U.S. Department of Energy, and Department of Chemistry, Iowa State University, Ames, Iowa, 50011

ARTICLE

ABSTRACT As noble metal nanoparticles are deployed into increasingly sophisticated environments, it is necessary to fully develop our understanding of nanoparticle behavior and the corresponding instrument responses. In this paper, we report on the optical response of three important gold nanorod configurations under dark field and differential interference contrast (DIC) microscopy after first establishing their absolute geometries with transmission electron microscopy (TEM). The observed longitudinal plasmon wavelengths of single nanorods are located at wavelengths consistent with previously developed theory. A dimer is shown exhibiting a multipole plasmon at wavelengths that are consistent with the dipole plasmon of single nanorods in the sample. DIC can also distinguish a single nanorod from a pair of uncoupled nanorods with an interparticle distance below the diffraction limit. The experimental observations are consistent with simulated DIC images using a DIC point spread function. The findings herein are a critical step toward being able to characterize nanorods in dynamic environments without the use of electron microscopy.

KEYWORDS: surface plasmon resonance · gold nanorod · diffraction limit · dark field microscopy · differential interference contrast (DIC) microscopy · multipole

Noble metal nanoparticles have quickly developed into an attractive probe for use in theoretical and analytical research. Owing to their plasmonic properties, nanoparticles can be readily detected with a variety of imaging techniques.[1−3] By simply adjusting the size, shape, or composition of a nanoparticle,[4−6] it is possible to design a nonfluorescent probe with a well-defined surface plasmon resonance (SPR) in the visible or near-infrared region of the spectrum. Furthermore, nanoparticles do not suffer from blinking or photobleaching,[7] and they can be imaged with a high temporal and spatial resolution.[2,3] Because of the aforementioned traits, nanoparticles can be utilized for observing either short-lived events or lengthy processes.

An important aspect of noble metal nanoparticles is that their optical response can be manipulated by environmental factors. For example, the position of the SPR can be influenced by the dielectric constants of the surrounding medium or the substrate.[8−11] The sensitivity to a dielectric substrate has been shown to be dependent on the level of contact between the particle and the substrate.[12] A single particle's SPR can also be affected by the presence of other nearby particles due to interparticle coupling of the plasmons. Coupling between two or more nanoparticles is highly dependent on the interparticle distance and the geometry of the interacting particles.[13−19]

The technique required for observing the optical response is often dependent on the application. Dark field microscopy is a popular method with high temporal resolution, and it is considered a benchmark for other modes of optical microscopy in imaging nanomaterials. Dark field images of nanoparticles resemble bright dots of light on a black background, because the microscope only collects the light that is scattered by the sample. To prevent any illuminating light from reaching the detector, the numerical aperture (NA) of the objective must be set smaller than the NA of the condenser.[12] Furthermore, dark field has decreased sensitivity in complex systems, such as cells,[20,21] because it must contend with scattering and distortions that arise from features along the optical path.[20]

Differential interference contrast (DIC) microscopy is a commercially available alternative to dark field microscopy. In the past, DIC has been used primarily for biological imaging, but it is gaining popularity as a tool in single particle research. DIC utilizes the principle of interferometry to produce high contrast images on a gray background. Because DIC utilizes a full NA at the objective, it supplies a higher lateral resolution and a shallower depth of field than dark field microscopy.[3] As a result, DIC is

*Address correspondence to nfang@iastate.edu.

Received for review September 22, 2010 and accepted November 18, 2010.

Published online November 23, 2010. 10.1021/nn102500s

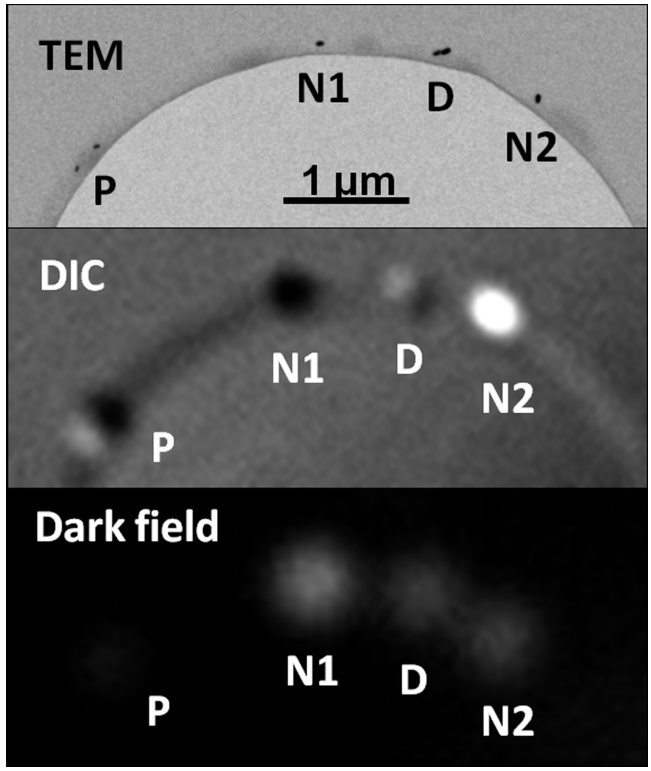

Figure 1. TEM, DIC, and dark field images of the four nanorod features investigated in this study. P: proximate nanorods; D: dimer; N1 and N2: single, isolated nanorods. All four features give different DIC intensity patterns.

capable of monitoring nanoparticles in complex environments, such as cells, for long periods of time with less interference from out-of-focus features.[22−24] However, the optical response of nanoparticles under DIC microscopy has not been correlated to the absolute configuration of the nanoparticle(s).

To address the aforementioned concern about DIC microscopy, we studied the optical response of three types of gold nanorod configurations under DIC and dark field microscopy. The optical responses were compared against observations collected with transmission electron microscopy (TEM). In the present study, isolated nanorods are defined as single rods separated by a distance greater than the diffraction limit, and they act independently of one another. Proximate neighbors is a new term used here to describe the case of two uncoupled nanorods with an interparticle distance below the diffraction limit. The proximate neighbors act independently, but the microscope detects a single point of light. Dimers consist of two interacting nanorods that are touching or nearly touching, and they have received much attention in recent papers. Depending on the sizes[13] and relative orientations[14,25] of the individual nanorods in a given dimer, it is possible for the individual longitudinal plasmons to couple and shift through electric field interactions.[26] In some instances, as the dipole plasmon red shifts, multipole peaks will emerge in the dimer's scattering spectrum.[27] Using a previously developed DIC point spread function,[28] a simulation was also employed to model the appearance of the DIC image. The simulation is designed for isolated nanoparticles and nanoparticles separated by a distance greater than 20 nm.

TABLE 1. Characteristics of the Four Features Studied[a]

feature	type	dimensions	aspect ratio	expected SPR (nm)
N1	single rod	63 nm × 32 nm	2.0	640
N2	single rod	78 nm × 37 nm	2.1	660
D	dimer		3.9−4.4	880−940
D-l		67 nm × 32 nm	2.1	660
D-r		77 nm × 36 nm	2.1	660
P	proximate rods			
P-l		48 nm ×23 nm	2.1	660
Pr		58 nm ×27 nm	2.2	670

[a]For the dimer and proximate nanorods, "l" and "r" refer to the individual nanorod that appears to the left or right of the feature's center point in the TEM images provided. The full length of the dimer was measured to be 141 nm. The center-to-center distance of the proximate nanorods was 227 nm (180 nm tip-to-tip). The expected position of the longitudinal SPR is calculated from eq 1. A range of aspect ratios was provided for the dimer, because the two nanorods are not aligned tip-to-tip.

RESULTS AND DISCUSSION

A UV−vis absorption spectrum was initially collected from the original gold colloid with a Varian Cary 300 UV−visible spectrophotometer. Between 400 and 900 nm, two absorption peaks appeared, with centers at 521 and 627 nm (Figure S1 in the Supporting Information). The peak at 627 nm is associated with the longitudinal axis, while the peak at 521 nm arises from the transverse axis. These values are reasonable for nanorods with an aspect ratio of ~2. At larger aspect ratios, the two SPR peaks are quite distinct in size, with the peak from the longitudinal axis dominating the spectrum.[29−31] As the aspect ratio approaches unity, the two peaks become similar in size and eventually merge.[32] However, the presence of particles of other shapes may also contribute to the 521 nm peak.[33] Sample polydispersity is also known to affect the actual peak positions, widths, and heights under UV−vis absorption.[29−31] As a result, electron microscopy must be relied upon for a more detailed characterization of the nanorods.

After applying an aliquot of the gold colloid to a holey carbon substrate, a distinct group of four nanorod features was located and characterized with a Philips CM-30 transmission electron microscope. It was quite fortuitous to locate these four features in one small area. TEM, DIC, and dark field images of the four features are shown in Figure 1, while the TEM-determined sizes of these features are reported in Table 1. Features N1 and N2 are single, isolated nanorods. Feature D is a nonoverlapping dimer with a total length of 141 nm. Feature P is a pair of proximate nanorods with a center-to-center interparticle distance of 227 nm (180 nm tip-to-tip). At wavelengths near the expected

longitudinal SPR (~660 nm) of feature P, the calculated diffraction limit (λ/2NA) is 236 nm, a value that is greater than the distance between P's two individual nanorods.

The expected dipolar longitudinal SPR wavelengths of the four features were calculated using the following equation:[29,34]

$$\lambda_{max} = (53.71R - 42.29)\varepsilon_m + 495.14 \qquad (1)$$

where λ_{max} is the longitudinal SPR wavelength; R is the aspect ratio; ε_m is 2.30, the dielectric constant of the Immersol 518F immersion oil from Zeiss that served as the surrounding medium. The calculated values are presented in Table 1. For the dimer, a range is given for the dipolar SPR wavelength, in order to reflect the different lengths of the two transverse axes involved.

By relying on the pattern recognition of permanent landmarks on the substrate, the same four nanorod features were located and inspected under dark field and DIC microscopy using a Nikon Eclipse 80i upright microscope. Once the features were located, the microscope's stage was rotated to find the angles that excited the longitudinal SPR of each feature. Under dark field microscopy with polarized illumination, an isolated nanorod produces its brightest intensity at the longitudinal SPR when its longitudinal axis is aligned with the polarizer; its weakest intensity occurs when the longitudinal axis is oriented perpendicular to the polarizer.[13,14,25,35] In comparison, DIC microscopy relies on a set of polarizers and Nomarski prisms. Before reaching the sample plane, the incoming light is split into two orthogonal wave fronts (Figure S2 in the Supporting Information).[36−39] When a nanorod's longitudinal axis is aligned with the bright wavefront, the nanorod appears entirely white. The nanorod is completely black in appearance when the nanorod is aligned with the dark wavefront. At angles in between the two wave fronts, nanorods take on a shadow-cast appearance.

Single, Isolated Nanorod. For the case of a single, isolated nanorod, images were collected over the range 500 to 780 nm using a Photometrics CoolSnap ES CCD camera. Under dark field conditions, the spectra of nanorod N1 were collected at the angles that excited the highest and lowest intensity at the longitudinal SPR wavelength, in following with the prior work of other researchers.[13,14,25,35] Intensity data were normalized in relation to the nanorod's highest observed intensity. Nanorod N1 has a longitudinal SPR peak at 660 nm un-

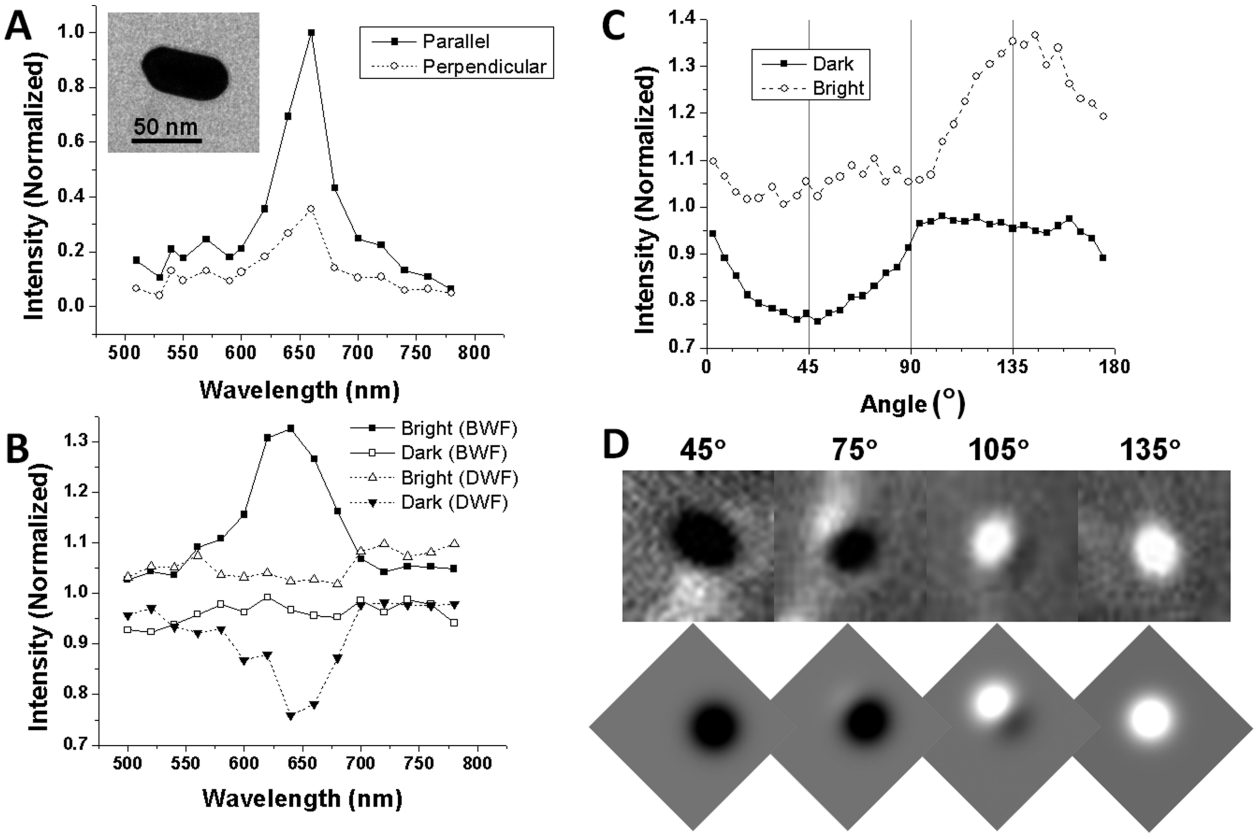

Figure 2. Profiles for isolated nanorod, N1. (A) Normalized dark field spectra with the longitudinal axis aligned parallel (solid line) and perpendicular (dashed) to the polarizer. Inset: TEM image of nanorod N1. (B) DIC intensity spectra at the bright and dark wave fronts. The mean background has a value of 1. BWF and DWF stand for bright and dark wave fronts, respectively. "Dark" and "Bright" refer to the intensity on the dark and bright sides of the nanorod. (C) DIC intensity profiles of the dark (solid) and bright (dashed) sides during 180° rotation in 5° increments at a wavelength of 640 nm. At 0°, 45°, and 135°, respectively, the nanorod is aligned with the polarizer, dark wavefront, and bright wavefront. (D) DIC images at 45°, 75°, 105°, and 135° (top), and DIC simulated images at the same angles (bottom).

der dark field conditions (Figure 2A). This peak appears at both particle orientations, and its intensity is greater when the longitudinal axis is aligned with the polarizer.

A perfect dipole should exhibit no longitudinal SPR peak when the nanorod is aligned perpendicular to the polarizer.[32,40] However, the coupling between a particle and the substrate can lead to a SPR that is predominantly, but not entirely, dipolar in nature.[10,26] In particular, as the aspect ratio of the nanorod decreases, the depolarization becomes more pronounced.[26]

Because of the shadow-cast appearance of nanorods at certain angles under DIC microscopy, it is possible to measure the intensity for both the bright and the dark portions of each particle as a function of the nanorod's angle under the DIC microscope. The intensity spectra for nanorod N1 were collected with the longitudinal axis aligned along both the bright and the dark wave fronts. The resultant spectra are presented in Figure 2B as they are related to the mean background intensity, which was assigned a value of 1. When the longitudinal axis is aligned with the bright wavefront, the nanorod's dark side intensity is close to the background intensity at all wavelengths, while a maximum in the bright side intensity appears near 645 nm, as predicted in Table 1. Likewise, when the nanorod is aligned with the dark wavefront, the bright side intensity is close to the background intensity, and the dark side intensity is significant at the longitudinal SPR. However, due to the working principle of DIC microscopy, the depolarized component is not involved in the image formation, and thus is not observed.[39]

Nanorod N1 was also observed at 640 nm, the longitudinal SPR wavelength, during a 180° rotation of the microscope's stage in 5° steps. The intensity profiles under rotation are shown in Figure 2C. At the angle 0°, the longitudinal axis is aligned with the polarizer; at 45°, the axis is parallel to the dark wavefront; at 135°, the axis is parallel to the bright wavefront. Both the bright and the dark side intensities exhibit a sinusoidal pattern. As expected, the nanorod's darkest and brightest intensities are centered at 45° (the dark wavefront) and 135° (the bright wavefront), respectively.

Figure 2D compares the observed and simulated DIC images that appear at 45°, 75°, 105°, and 135° for the nanorod rotation in Figure 2C. When a nanorod is aligned with the dark wavefront, the simulation produces a particle that is entirely black in appearance. As nanorods are rotated away from the dark wavefront, they take on a slowly increasing bright side component at the expense of the dark side. Once aligned with the bright wavefront, the dark side disappears completely, and the particle's appearance is completely white. These simulated results agree well with the observed behavior of the single nanorod, N1.

The behavior of nanorod N2 (Figure S3 in the Supporting Information) was similar, but not identical, to that of N1, as expected.[41] As predicted in Table 1, DIC microscopy found that the longitudinal SPR for N2 was red-shifted in comparison to the SPR for N1.

Proximate Nanorods. Feature P is a pair of nanorods with an interparticle distance of 227 nm, and the angle between the two longitudinal axes is ~120°. Images of feature P were collected from 500 to 780 nm using the Photometrics CoolSnap ES CCD camera. On the basis of the sizes of the nanorods and their interparticle distance, the effects of interparticle coupling were expected to be minimal.[25,42] However, because the interparticle distance is less than the diffraction limit, optical microscopy detects a single, convoluted particle image.

Using dark field microscopy, the spectra were collected with the interparticle axis aligned either parallel or perpendicular to the polarizer. The spectra presented a maximum in intensity at 660 nm for both orientations (Figure 3A). The intensity was greater in value when the interparticle axis was aligned parallel to the polarizer, because the longitudinal axes of both nanorods are well-aligned with the polarizer at this angle, as demonstrated in the Figure 3A inset. When the interparticle axis was rotated by 90°, a longitudinal component of each nanorod was still aligned with the two wave fronts, and a small peak was observed in the spectrum. The dark field spectra of the proximate nanorods thus resembled those of a single nanorod.

In the DIC mode, spectra were collected while the interparticle axis was aligned either parallel or perpendicular to the polarizer. At these angles, the two nanorods are well-aligned with the two DIC wave fronts (see Figure 3B,inset), and the DIC image has a significant bright side and dark side component (Figure 3B). A closer inspection of the spectra reveals that each pair of bright and dark intensity profiles has slightly offset peak positions. For example, when the interparticle axis is aligned perpendicular to the polarizer (the solid curves in Figure 3B), we find a bright-side intensity maximum at 660 nm and a dark-side intensity maximum at 680 nm, clearly demonstrating the contributions from the two individual nanorods. When the interparticle axis is aligned parallel to the polarizer, the dark-side maximum is now at 660 nm, and the bright-side maximum is at 680 nm. At both angles, the peak at 660 nm is considerably stronger than the peak at 680 nm, thus demonstrating a difference in scattering abilities.

Feature P was observed during a 360° rotation under DIC microscopy at 680 nm, and it was found that the intensity profiles were dependent on the orientation of the interparticle axis (Figure 3C). However, the DIC rotational profile of the proximate nanorods is more complex than the profile observed with N1. Maxima in the contrast (the difference in intensity between the bright and the dark sides) appear near 180° and 270°, with minor maxima appearing near 0° and 90°. These four angles coincide with the interparticle axis being aligned parallel (0° and 180°) or perpendicular (90° and

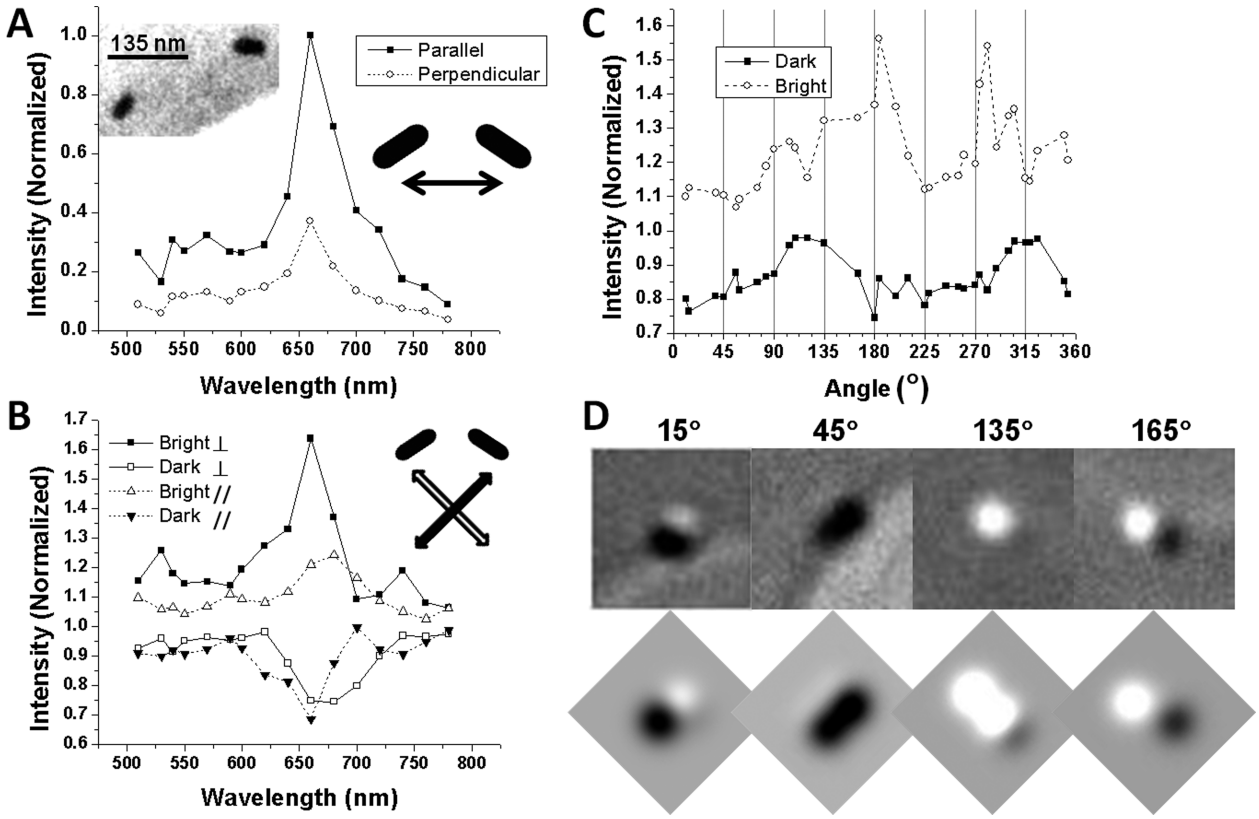

Figure 3. Profiles for proximate nanorods, P. (A) Normalized dark field spectra with the interparticle axis aligned parallel (solid) and perpendicular (dashed) to the polarizer. Insets: TEM image of P, and schematic of optimal nanorod alignment with the polarizer (arrow). (B) DIC intensity spectra with the interparticle axis aligned perpendicular (90°, ⊥) and parallel (180°, ∥) to the polarizer. Inset: Schematic of optimal nanorod alignment with the wave fronts under DIC microscopy. (C) DIC intensity profiles under a full 360° rotation at 680 nm. (D) DIC images (above) and simulations (below) with the interparticle axis at angles of 15°, 45°, 135°, and 165°.

270°) to the polarizer. The profile does not have the sinusoidal shape that was found with N1.

On the basis of these observations, it is possible to conjecture as to how the convoluted contrast would change as the relative orientation of two identical nanorods in a proximate configuration is altered. If two proximate nanorods were aligned tip-to-tip or side-by-side, the individual plasmons would exhibit equivalent optical behavior as they were rotated on the stage. At the other extreme, if the two nanorods were aligned at 90° angles to each other, a total of four distinct maxima should appear in the bright side (and the dark side) intensity profile during a full rotation of the feature. With the latter orientation, the maximum bright side and dark side intensities would always appear at the same angles. As the nanorods go from a parallel to a perpendicular orientation, the intensity maxima should gradually broaden and eventually split into four peaks. Moreover, at these intermediate interparticle angles, the feature is always partially aligned with both DIC wave fronts, regardless of the feature's orientation angle. Because feature P includes two nanorods at different aspect ratios and with different scattering abilities, its rotational behavior is further complicated, yet its optical behavior remains quite distinct from that of the single nanorod, N1.

The DIC simulation was utilized to model the proximate nanorods, and the simulated images were compared to the actual DIC images (Figure 3D). At most angles, the dark and bright sides remain apparent simultaneously in both sets of images. As the interparticle axis comes into alignment with either of the wave fronts (45°, 135°), the simulated image takes on an appearance that is almost entirely white or black, as with the actual image.

Nanorod Dimer. To explain the observed behavior of feature D, the dimer, it is first necessary to review some of the other recent work in this area. As two individual nanoparticles are brought together, their plasmons interact and hybridize, resulting in a red shift in the longitudinal SPR wavelength. The plasmon shift remains negligible for a pair of parallel particles that are separated by distances greater than 2.5 times the length of the nanorod's transverse axis.[42] For other nanorod orientations, the reach of the plasmon interaction is highly variable.[25]

When a pair of nanorods interact and couple at relatively long interparticle distances (d), their plasmons behave as classical dipoles and shift according to $1/d^3$, while at relatively short distances, the plasmon shift depends on $1/d$.[16,43] More recently, dimer plasmons have been studied at extremely short interparticle distances,

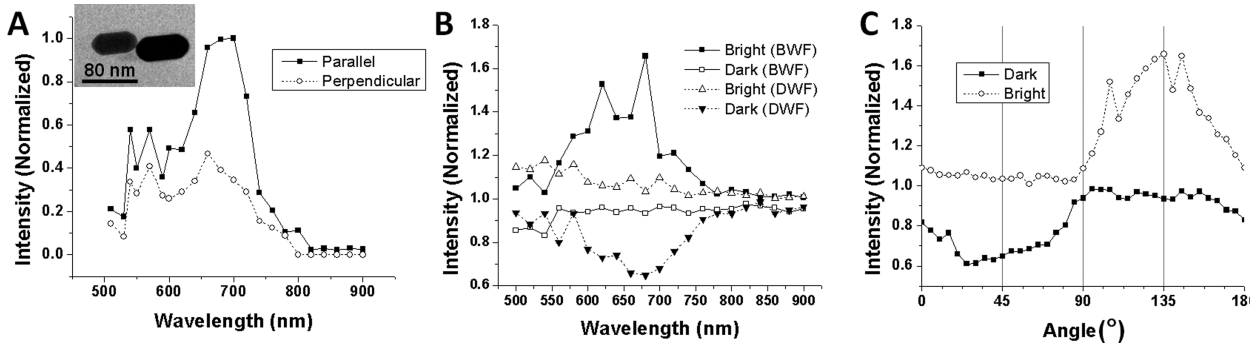

Figure 4. Profiles for the dimer, D. (A) Normalized dark field spectra with the interparticle axis aligned parallel and perpendicular to the polarizer. Inset: TEM image of feature D. (B) DIC intensity spectra with the interparticle axis aligned parallel to the bright and dark wave fronts. (C) DIC intensity profiles from 180° rotation in 5° increments at 680 nm.

where the separation to rod length ratios are below 0.09.[14,27,44] In this near-contact regime, shifting of the dipole plasmon does not follow the aforementioned theory. Instead, the geometry of the junction between the two particles becomes critical in the extent of the plasmon shift.[19]

As two particles approach each other toward a single point of contact within the near-contact regime, the dipole peak becomes narrower and undergoes enhanced red shifting.[19,27,45] To compensate for the decreased scattering by the dipole, additional peaks emerge at shorter wavelengths through the interactions of multipoles. As the interparticle distance is further decreased, the dimer's multipole peaks will also red shift and gradually decrease in size, while the dipole peak can disappear completely.[27]

According to the calculation used in Table 1, the dimer was expected to have a longitudinal SPR located between 880 and 940 nm. In the TEM image (Figure 4A inset), the surfaces of the two nanorods appear to be within 1 nm of each other. The presence of surfactant molecules at the surface of the two nanorods could easily prevent the two gold surfaces from making actual contact. Assuming the nanorods are not touching, the dimer fits in the near-contact region, because it has a separation to rod length ratio below 0.015.

Feature D was initially examined from 500 to 780 nm with the Photometrics CoolSnap ES CCD camera, because of its high resolution. At longer wavelengths, the data was collected with a Photometrics Evolve CCD camera, since the Evolve has higher quantum efficiency in this region than the CoolSnap ES. Dark field spectra were collected with the interparticle axis aligned both parallel to and perpendicular to the polarizer. Dark field microscopy detected a strong SPR peak between 640 and 720 nm, as shown in Figure 4A. The peak here was broader than that of the single nanorods, and the intensity at shorter wavelengths (540−620 nm) was also increased. At wavelengths longer than 750 nm, the observed intensity was weak at both particle orientations.

The full DIC spectra collected for the dimer are presented in Figure 4B. Broad regions of resonance occur between 620 and 720 nm, with a maximum at 680 nm. The expected dipole longitudinal SPR near 900 nm was not observed. On the basis of the prior work of other research groups,[19,45] we believe that the dipole SPR was either red-shifted beyond 900 nm, or more likely, it disappeared as a result of the near-contact coupling. The peak at 680 nm should be from a multipolar resonance.

Figure 4B reveals that the dimer is entirely white in appearance from 620 to 740 nm when the dimer is aligned with the bright wavefront, and it is completely black over the same region when aligned with the dark wavefront. Figure 4C displays the DIC rotational profiles collected for the dimer's multipole at 680 nm. The data reveal that the darkest and brightest intensities are centered around 45° and 135°. The rotational profile exhibits a pattern similar to that of the single nanorod, N1.

To summarize, we have reported on the optical response of three gold nanorod configurations under DIC microscopy after obtaining a precise characterization of the nanorods with TEM. Such fundamental work is of importance to the basic understanding of nanorod behavior, particularly for single-particle tracking experiments and other dynamic environments where electron microscopy cannot be applied. Because of the presence of two wave fronts in DIC microscopy, DIC provides an added dimension to the observation of gold nanorods in comparison to dark field microscopy. This added dimension is especially influential when looking at the dimer and the proximate nanorod configurations.

The results herein also suggest that single particles cannot always be distinguished from other configurations by simply inspecting the sample at a single wavelength or at a single observation angle. Multipoles from dimers can prove problematic, because they can appear at or near the wavelengths where a single nanorod's dipole SPR is expected. Proximate nanorods can be likewise troublesome. DIC's added dimensionality was able to reveal the presence of two nanorods for the proximate configuration encountered here, and DIC microscopy should be able to distinguish most proxi-

mate nanorod configurations from a single nanorod, unlike dark field microscopy. The results here also stress the importance of investigating additional nanorod configurations with DIC microscopy.

MATERIALS AND METHODS

Materials and Sample Preparation. The hemispherically capped gold nanoparticles used in this study were purchased from Nanopartz as a colloidal suspension (Salt Lake City, UT). Before applying gold nanoparticles to the substrate, 50 μL of the gold colloid were centrifuged at 5500 rpm for 10 min, resuspended in 15 μL of Milli-Q water, and sonicated for 20 min. This process removed excess surfactant from the solution. The substrate was a TEM grid made of holey carbon and backed by a 200-mesh copper grid (SPI Supplies, West Chester, PA). This substrate was selected, because holey carbon is known for its stability under an electron beam. Holey carbon is known to be dielectric, but the exact dielectric constant of the substrates used in this study is unknown. The circular substrate had an outer diameter of 3.05 mm, and each grid square was 97 μm × 97 μm. After setting the substrate on Whatman filter paper, 5 μL of the gold colloid were applied to the substrate and allowed to dry.

After the sample was first analyzed by TEM, the substrate was prepared for optical microscopy. The substrate was placed on 25 × 75 × 1 mm^3 precleaned microscope slide from Fisher Scientific (Pittsburgh, PA). Next, the substrate was suspended in Carl Zeiss Immersol 518F immersion oil (Thornwood, NY), which has a refractive index of 1.518. The sample was immediately covered with a No. 1 coverslip from Corning (Corning, NY). Single-sided and double-sided tapes were utilized to hold the coverslip in place.

Transmission Electron Microscopy. A Philips CM-30 transmission electron microscope operating at 200 kV was used for collecting the TEM data. Images were collected with a Gatan Orius SC 1000 CCD camera at an 11 Megapixel (4008 × 2672) resolution using Gatan DigitalMicrograph. ImageJ was used to determine the size and orientation of the nanorods observed. All measurements were collected multiple times, and the mean values were reported herein.

Optical Microscopy. All optical microscopy was completed with a Nikon Eclipse 80i upright microscope equipped with a 12 V−100 W halogen lamp. A Photometrics CoolSnap ES CCD camera (1392 × 1040 pixel imaging array) was utilized for images collected between 500 and 780 nm due to its high resolution capabilities. Above 780 nm, a Photometrics Evolve CCD camera (512 × 512 pixel imaging array) was employed due to its greater quantum efficiency at longer wavelengths. At intermediate wavelengths (600−800 nm), the two cameras yielded similar particle spectra. In both the dark field and DIC modes, the microscope's zoom knob was set to 1.6×, and a 100× objective was used.

To collect data at specified wavelengths, a set of bandpass filters from Thorlabs, Inc. (Newton, NJ) were employed. Each filter had a central wavelength in the range of 500−900 nm and a full width at half-maximum (fwhm) bandpass region equivalent to 10 nm. Filters were placed between the condenser and the sample slide. The sample slide was supported by a rotating stage, and the actual orientation of the slide was determined by focusing the microscope on the copper grid. The nanorods of interest were readily found after each rotation of the stage through the use of permanent and easily identifiable landmarks on the substrate. All data were analyzed with ImageJ.

In dark field mode, the microscope utilized a Nikon Plan Fluor 100× 0.5−1.3 oil iris objective with its numerical aperture (NA) set to 0.7 and a Nikon dark field condenser with a 1.43−1.20 NA in oil. A polarizer was placed between the condenser and the bandpass filter. To excite the brightest intensity of a single nanorod, the longitudinal axis was aligned parallel to the polarizer. The darkest intensity was examined by orienting the longitudinal axis perpendicular to the polarizer. For the dimer and for spaced nanorods, the two modes were studied by aligning the interparticle axis either parallel or perpendicular to the polarizer. In image analysis, a circular area immediately adjacent to each feature was chosen for the background readings for both DIC and dark field microscopies.

The differential interference contrast (DIC) mode required a Nomarski prism and polarizer on either side of the sample plane, as well as a Nikon 100× 1.40 NA Plan Apo VC oil immersion objective and a 1.40 NA Nikon oil immersion condenser.[36−38] Because the prism is oriented at a 45° angle to the polarizer, the two wave fronts are oriented at 45° and 135° to the polarizer. The bright and dark modes of a nanorod are examined by aligning the nanorod's longitudinal axis along one of the wave fronts, not the polarizer. After the wave fronts pass through the sample plane, they are recombined by the second Nomarski prism (oriented at 135° to the polarizer) before exiting through the analyzer (oriented perpendicular to the polarizer). By combining the two wave fronts, an interference pattern is generated, and objects such as nanoparticles take on a 3-dimensional shadow appearance with a bright side and a dark side. Thus, DIC can be used to collect either intensity or contrast data.

DIC Simulation. A home-written C++ computer program using an established DIC point spread function[28] was utilized to simulate a single nanoparticle or a pair of nanoparticles separated by at least 20 nm. The simulation represents the expected 2D DIC image at the longitudinal SPR wavelength. The shape, size, location, and orientation of the nanoparticle(s) were read into the program before running each simulation. DIC images of the nanoparticle(s) were output as a 1 μm × 1 μm matrix with grid spacing of 10 nm.

The DIC point spread function is a function of the shear distance, the phase bias applied on the two illumination beams, and the point spread function for the transmitted light optics under coherent illumination of the microscope.[28] In the simulation, the shear distance was assumed to be 100 nm. The phase bias was assumed to be 90°. The phase delays of the ordinary and the extraordinary illumination beams caused by the nanorod were assumed to be 0° and 30°, respectively. A 2D Gaussian approximation was utilized to model the point spread function of the transmission microscope. With our microscope, single subdiffraction limit particles have an apparent diameter of ~600 nm at a wavelength of 660 nm. Assuming the particle image represents the 99% confidence limits for the true central position of the particle, the image has a width of 6σ. As a result, σ is approximately 100 nm. This value agreed well with the equation for the paraxial point spread function of a wide-field fluorescence microscope that imposes peak matching, $\sigma = 0.21\lambda/NA$.[46] For the case of $\lambda = 660$ nm and NA = 1.40, σ is equivalent to 99 nm.

Acknowledgment. The Ames Laboratory is operated for the U.S. Department of Energy by Iowa State University under Contract No. DE-AC02-07CH11358. This work was supported by the Chemical Sciences, Geosciences, and Biosciences Division, Basic Energy Sciences, Office of Science, U.S. Department of Energy. The authors wish to thank Drs. Yaqiao Wu and Matthew Kramer for kindly providing assistance on the TEM work.

Supporting Information Available: Detailed figures of nanorod, N2; a figure of the UV−vis absorption spectra and a figure detailing the proper nanorod alignment under dark field and DIC microscopy. This material is available free of charge *via* the Internet at http://pubs.acs.org.

REFERENCES AND NOTES

1. De, M.; Ghosh, P. S.; Rotello, V. M. Applications of Nanoparticles in Biology. *Adv. Mater.* **2008**, *20*, 4225–4241.
2. Murphy, C. J.; Gole, A. M.; Stone, J. W.; Sisco, P. N.; Alkilany, A. M.; Goldsmith, E. C.; Baxter, S. C. Gold Nanoparticles in Biology: Beyond Toxicity to Cellular Imaging. *Acc. Chem. Res.* **2008**, *41*, 1721–1730.

3. Wang, G. F.; Stender, A. S.; Sun, W.; Fang, N. Optical Imaging of Non-fluorescent Nanoparticle Probes in Live Cells. *Analyst* **2010**, *135*, 215–221.
4. El-Sayed, M. A. Some Interesting Properties of Metals Confined in Time and Nanometer Space of Different Shapes. *Acc. Chem. Res.* **2001**, *34*, 257–264.
5. Kelly, K. L.; Coronado, E.; Zhao, L. L.; Schatz, G. C. The Optical Properties of Metal Nanoparticles: The Influence of Size, Shape, and Dielectric Environment. *J. Phys. Chem. B* **2002**, *107*, 668–677.
6. Mulvaney, P. Not All That's Gold Does Glitter. *MRS Bull.* **2001**, *26*, 1009–1014.
7. Sonnichsen, C.; Reinhard, B. M.; Liphardt, J.; Alivisatos, A. P. A Molecular Ruler Based on Plasmon Coupling of Single Gold and Silver Nanoparticles. *Nat. Biotechnol.* **2005**, *23*, 741–745.
8. Haynes, C. L.; Van Duyne, R. P. Nanosphere Lithography: A Versatile Nanofabrication Tool for Studies of Size-Dependent Nanoparticle Optics. *J. Phys. Chem. B* **2001**, *105*, 5599–5611.
9. Jain, P. K.; El-Sayed, M. A. Noble Metal Nanoparticle Pairs: Effect of Medium for Enhanced Nanosensing. *Nano Lett.* **2008**, *8*, 4347–4352.
10. Knight, M. W.; Wu, Y.; Lassiter, J. B.; Nordlander, P.; Halas, N. J. Substrates Matter: Influence of an Adjacent Dielectric on an Individual Plasmonic Nanoparticle. *Nano Lett.* **2009**, *9*, 2188–2192.
11. Novo, C.; Funston, A. M.; Pastoriza-Santos, I.; Liz-Marzan, L. M.; Mulvaney, P. Influence of the Medium Refractive Index on the Optical Properties of Single Gold Triangular Prisms on a Substrate. *J. Phys. Chem. C* **2007**, *112*, 3–7.
12. McMahon, J. M.; Wang, Y.; Sherry, L. J.; Van Duyne, R. P.; Marks, L. D.; Gray, S. K.; Schatz, G. C. Correlating the Structure, Optical Spectra, and Electrodynamics of Single Silver Nanocubes. *J. Phys. Chem. C* **2009**, *113*, 2731–2735.
13. Brown, L. V.; Sobhani, H.; Lassiter, J. B.; Nordlander, P.; Halas, N. J. Heterodimers: Plasmonic Properties of Mismatched Nanoparticle Pairs. *ACS Nano* **2010**, *4*, 819–832.
14. Funston, A. M.; Novo, C.; Davis, T. J.; Mulvaney, P. Plasmon Coupling of Gold Nanorods at Short Distances and in Different Geometries. *Nano Lett.* **2009**, *9*, 1651–1658.
15. Hentschel, M.; Saliba, M.; Vogelgesang, R.; Giessen, H.; Alivisatos, A. P.; Liu, N. Transition from Isolated to Collective Modes in Plasmonic Oligomers. *Nano Lett.* **2010**, *10*, 2721–2726.
16. Nordlander, P.; Oubre, C.; Prodan, E.; Li, K.; Stockman, M. I. Plasmon Hybridization in Nanoparticle Dimers. *Nano Lett.* **2004**, *4*, 899–903.
17. Shao, L.; Woo, K. C.; Chen, H.; Jin, Z.; Wang, J.; Lin, H.-Q. Angle- and Energy-Resolved Plasmon Coupling in Gold Nanorod Dimers. *ACS Nano* **2010**, *4*, 3053–3062.
18. Sheikholeslami, S.; Jun, Y.-w.; Jain, P. K.; Alivisatos, A. P. Coupling of Optical Resonances in a Compositionally Asymmetric Plasmonic Nanoparticle Dimer. *Nano Lett* **2010**, *10*, 2655–2660.
19. Zuloaga, J.; Prodan, E.; Nordlander, P. Quantum Description of the Plasmon Resonances of a Nanoparticle Dimer. *Nano Lett.* **2009**, *9*, 887–891.
20. Tsunoda, M.; Isailovic, D.; Yeung, E. S. Real-Time Three-Dimensional Imaging of Cell Division by Differential Interference Contrast Microscopy. *J. Microsc.,Oxford* **2008**, *232*, 207–211.
21. Chang, W.-S.; Ha, J. W.; Slaughter, L. S.; Link, S. Plasmonic Nanorod Absorbers as Orientation Sensors. *Proc. Nat. Acad. Sci. U.S.A.* **2010**, *107*, 2781–2786.
22. Sun, W.; Fang, N.; Trewyn, B. G.; Tsunoda, M.; Slowing, I. I.; Lin, V. S. Y.; Yeung, E. S. Endocytosis of a Single Mesoporous Silica Nanoparticle into a Human Lung Cancer Cell Observed by Differential Interference Contrast Microscopy. *Anal. Bioanal. Chem.* **2008**, *391*, 2119–2125.
23. Sun, W.; Wang, G.; Fang, N.; Yeung, E. S. Wavelength-Dependent Differential Interference Contrast Microscopy: Selectively Imaging Nanoparticle Probes in Live Cells. *Anal. Chem.* **2009**, *81*, 9203–9208.
24. Luo, Y.; Sun, W.; Gu, Y.; Wang, G. F.; Fang, N. Wavelength-Dependent Differential Interference Contrast Microscopy: Multiplexing Detection Using Nonfluorescent Nanoparticles. *Anal. Chem.* **2010**, *82*, 6675–6679.
25. Tabor, C.; Van Haute, D.; El-Sayed, M. A. Effect of Orientation on Plasmonic Coupling between Gold Nanorods. *ACS Nano* **2009**, *3*, 3670–3678.
26. Vernon, K. C.; Funston, A. M.; Novo, C.; Gomez, D. E.; Mulvaney, P.; Davis, T. J. Influence of Particle-Substrate Interaction on Localized Plasmon Resonances. *Nano Lett.* **2010**, *10*, 2080–2086.
27. Romero, I.; Aizpurua, J.; Bryant, G. W.; García De Abajo, F. J. Plasmons in Nearly Touching Metallic Nanoparticles: Singular Response in the Limit of Touching Dimers. *Opt. Express* **2006**, *14*, 9988–9999.
28. Preza, C.; Snyder, D. L.; Conchello, J. A. Theoretical Development and Experimental Evaluation of Imaging Models for Differential-Interference-Contrast Microscopy. *J. Opt. Soc. Am. A* **1999**, *16*, 2185–2199.
29. Link, S.; Mohamed, M. B.; El-Sayed, M. A. Simulation of the Optical Absorption Spectra of Gold Nanorods as a Function of Their Aspect Ratio and the Effect of the Medium Dielectric Constant. *J. Phys. Chem. B* **1999**, *103*, 3073–3077.
30. Becker, J.; Zins, I.; Jakab, A.; Khalavka, Y.; Schubert, O.; Sonnichsen, C. Plasmonic Focusing Reduces Ensemble Linewidth of Silver-Coated Gold Nanorods. *Nano Lett.* **2008**, *8*, 1719–1723.
31. Link, S.; Mohamed, M.; El-Sayed, M. Simulation of the Optical Absorption Spectra of Gold Nanorods as a Function of Their Aspect Ratio and the Effect of the Medium Dielectric Constant. *J. Phys. Chem. B* **1999**, *103*, 3073–3077.
32. Sonnichsen, C.; Franzl, T.; Wilk, T.; von Plessen, G.; Feldmann, J.; Wilson, O. Drastic Reduction of Plasmon Damping in Gold Nanorods. *Phys. Rev. Lett.* **2002**, *88*, 077402.
33. Muskens, O. L.; Bachelier, G.; Del Fatti, N.; Vallee, F.; Brioude, A.; Jiang, X. C.; Pileni, M. P. Quantitative Absorption Spectroscopy of a Single Gold Nanorod. *J. Phys. Chem. C* **2008**, *112*, 8917–8921.
34. Link, S.; El-Sayed, M. A. Simulation of the Optical Absorption Spectra of Gold Nanorods as a Function of Their Aspect Ratio and the Effect of the Medium Dielectric Constant. *J. Phys. Chem. B* **2005**, *109*, 10531–10532.
35. Slaughter, L. S.; Chang, W.-S.; Swanglap, P.; Tcherniak, A.; Khanal, B. P.; Zubarev, E. R.; Link, S. Single-Particle Spectroscopy of Gold Nanorods Beyond the Quasi-static Limit: Varying the Width at Constant Aspect Ratio. *J. Phys. Chem. C* **2010**, *114*, 4934–4938.
36. Lessor, D. L.; Hartman, J. S.; Gordon, R. L. Quantitative Surface-Topography Determination by Nomarski Reflection Microscopy. 1. Theory. *J. Opt. Soc. Am.* **1979**, *69*, 357–366.
37. Lang, W. Nomarski Differential Interference Contrast Microscopy. *Zeiss Info.* **1968**, *70*, 114–120.
38. Padawer, J. The Nomarski Interference-Contrast Microscope, an Experimental Basis for Image Interpretation. *J. R. Microsc. Soc.* **1968**, *88*, 305–349.
39. Wang, G.; Sun, W.; Luo, Y.; Fang, N. Resolving Rotational Motions of Nano-objects in Engineered Environments and Live Cells with Gold Nanorods and Differential Interference Contrast Microscopy. *J. Am. Chem. Soc.* **2010**, *132*, 16417–16422.
40. Pelton, M.; Liu, M. Z.; Park, S.; Scherer, N. F.; Guyot-Sionnest, P. Ultrafast Resonant Optical Scattering from Single Gold Nanorods: Large Nonlinearities and Plasmon Saturation. *Phys. Rev. B* **2006**, *73*, 155419.
41. Tcherniak, A.; Ha, J. W.; Dominguez-Medina, S.; Slaughter, L. S.; Link, S. Probing a Century Old Prediction One Plasmonic Particle at a Time. *Nano Lett.* **2010**, *10*, 1398–1404.

42. Su, K. H.; Wei, Q. H.; Zhang, X.; Mock, J. J.; Smith, D. R.; Schultz, S. Interparticle Coupling Effects on Plasmon Resonances of Nanogold Particles. *Nano Lett.* **2003**, *3*, 1087–1090.
43. Haynes, C. L.; McFarland, A. D.; Zhao, L.; Van Duyne, R. P.; Schatz, G. C.; Gunnarsson, L.; Prikulis, J.; Kasemo, B.; Kall, M. Nanoparticle Optics: The Importance of Radiative Dipole Coupling in Two-Dimensional Nanoparticle Arrays. *J. Phys. Chem. B* **2003**, *107*, 7337–7342.
44. Claro, F. Absorption Spectrum of Neighboring Dielectric Grains. *Phys. Rev. B* **1982**, *25*, 7875.
45. Atay, T.; Song, J.-H.; Nurmikko, A. V. Strongly Interacting Plasmon Nanoparticle Pairs: From Dipole−Dipole Interaction to Conductively Coupled Regime. *Nano Lett.* **2004**, *4*, 1627–1631.
46. Zhang, B.; Zerubia, J.; Olivo-Marin, J. C. Gaussian Approximations of Fluorescence Microscope Point-Spread Function Models. *Appl. Opt.* **2007**, *46*, 1819–1829.